

**Ilmenite and amorphous SnTiO₃ as *p*-type oxide semiconductor**

Journal:	<i>Journal of Materials Chemistry C</i>
Manuscript ID	TC-ART-11-2022-004937.R1
Article Type:	Paper
Date Submitted by the Author:	28-Feb-2023
Complete List of Authors:	Hu, Yaoqiao; The University of Texas at Dallas, ; The Hong Kong University of Science and Technology, Schlom, Darrell; Cornell University Datta, Suman; Georgia Institute of Technology, School of Electrical and Computer Engineering Cho, Kyeongjae; The University of Texas at Dallas,

Ilmenite and amorphous SnTiO₃ as *p*-type oxide semiconductor

Yaoqiao Hu¹, Darrell Schlom^{2,3}, Suman Datta⁴, and Kyeongjae Cho¹

¹Department of Materials Science and Engineering, The University of Texas at Dallas, Richardson, Texas 75080, USA

²Department of Materials Science and Engineering, Cornell University, Ithaca, New York 14853-1501, USA

³Kavli Institute at Cornell for Nanoscale Science, Ithaca, New York 14853, USA

⁴School of Electrical and Computer Engineering, Georgia Institute of Technology, Atlanta, Georgia 30332, USA

Corresponding Author: Kyeongjae Cho. Email: kjcho@utdallas.edu

Abstract

A Sn²⁺ based oxide, ilmenite SnTiO₃, is investigated as a potential *p*-type oxide. Due to Sn²⁺ chemistry, ilmenite SnTiO₃ shows dispersive valence band with a wide band gap of 2.4 eV and high hole mobility of ~60 cm²/(V·s). Thermodynamics study confirms its phase stability and synthesizability. Defect calculation demonstrates its high hole dopability. Further band alignment calculation shows its shallow valence band edge suitable for metal contact. Amorphous phase SnTiO₃ is revealed to be a high mobility hole-dopable oxide. The results suggest ilmenite and amorphous SnTiO₃ is an experimentally realizable *p*-type oxide promising for future oxide electronics.

1. Introduction

Oxide semiconductors, due to their atmospheric stability, ease of synthesis, and wide band gap, have been widely used as semiconducting channel materials and transparent conducting oxide electrodes in various electronic and optoelectronic devices.¹⁻⁴ Recently, they have been proposed as the back-end-of-line (BEOL) compatible transistor channel materials for implementing vertical CMOS technology.⁵⁻⁷ Until now most available oxide semiconductors are *n*-type oxides, for instance, In₂O₃, ITO, and IGZO, whereas their *p*-type counterparts remain scarce. This dominance of *n*-type oxides is because of the fundamental electronic structures associated with oxides: the top valence bands in typical oxides are dominated by deep-lying (8-9 eV below the vacuum level) and localized oxygen-2*p* orbitals which result in limited hole mobility and hole doping.^{8, 9} Over the last decade, substantial research works have been reported on searching for high mobility and hole dopable *p*-type oxides to expand *p*-type oxides materials library for future realization of complementary *n*-type and *p*-type oxide electronics.⁹⁻¹²

In our recent works, the main strategy of designing *p*-type oxides with high performance, i.e., high hole mobility and good hole dopability, is to alleviate the dominance of O-2*p* orbital at the valence band edge (VBE) by introducing additional shallower and more extended orbital states above O-2*p* orbital.^{8, 9} Such occupied orbital states should be compatible with O-2*p* in terms of both energy position and symmetry to maximize the orbital hybridization. A previous work has identified three groups of orbitals that can achieve this strategy: (i) *d* orbitals from transition metals, (ii) lone-pair *s* orbitals from post transition metals, and (iii) *p* orbitals from non-oxygen anions.¹¹ Historically, *p*-type oxide searches are concentrated on transition metal-based oxides such as Cu₂O, CuAlO₂ and NiO.¹³⁻¹⁵ Later, *p*-type oxide studies are shifted to lone-pair *s* orbital oxides when Hosono reported SnO *p*-channel transistor.¹⁶ Starting from early 2010s, high-throughput materials screening has identified more *p*-type oxide materials space including Sn²⁺, Bi³⁺, Tl¹⁺, Sb³⁺, and Pb²⁺, etc.¹⁰ Non-oxygen anion *p*-orbital based *p*-type oxides are still in the early stage of investigation and only a few of them from this group have been theoretically identified (e.g., LaCuOSe¹¹, ZrOS¹⁰) while experimentally not yet demonstrated.

In our previous work, we have focused on Sn²⁺ chemistry and searched for Sn²⁺ based *p*-type oxides where the orbital hybridization between Sn-5*s* and O-2*p* at the valence band edge (VBE) drives a light hole effective mass.⁹ This search has led to the identification of several promising *p*-type oxides including Ta₂SnO₆ and SnTiO₃.⁹ While we have performed experimental demonstration of Ta₂SnO₆ as a *p*-type oxide¹⁷, little attention has been given to SnTiO₃. In this work, we present a systematic investigation on SnTiO₃ potential for *p*-type oxide. SnTiO₃ occurs in two distinct polymorphs: perovskite and ilmenite. Our previous work has revealed that ilmenite SnTiO₃ is the more stable polymorph.⁹ Recent work reporting a successful synthesis of ilmenite SnTiO₃ demonstrates that SnTiO₃ is an experimental achievable *p*-type oxide.^{18, 19} We study the *p*-type oxide performance of SnTiO₃ by examining its phase stability, carrier mobility, and *p*-doping dopability in both ilmenite and amorphous phases. Our results show that SnTiO₃ possess a decent

hole mobility and high p -type dopability, which can serve as an experimental realizable p -type oxide for future oxide electronics.

II. Computational methods

All theoretical calculations reported in this work were carried out by using density functional theory (DFT) based first principles calculations, as implemented in Vienna Ab initio Simulation Package (VASP). Projector augmented wave (PAW) method²⁰ and plane wave basis set were used. For electron exchange-correlation interaction, hybrid function of Heyd–Scuseria–Ernzerhof (HSE) type²¹ was employed. A cutoff energy of 520 eV was adopted throughout all calculations. For electronic structure calculation, primitive cell was used with a $6\times 6\times 6$ Gamma-centered k -point mesh grid for Brillouin zone sampling. The criterion for self-consistent electronic minimization is total energy converging at 10^{-5} eV. For band alignment calculation, slab model was used to determine the valence band edge position relative to the vacuum level.^{22, 23} Chemical potential phase diagram was calculated based on DFT-determined formation energy. Detailed procedure of generating chemical potential map can be found in Ref [9]. Defect computation was based on supercell to minimize the interaction between charged defects and their periodic images. Energy correction was performed by using Freysoldt scheme²⁴, as implemented in the PyCDT package.²⁵

III. Results and discussion

Stable SnTiO_3 phase adopts the structure similar to FeTiO_3 ilmenite (rhombohedral space group, $R\bar{3}$, #148). The lattice parameters for the ilmenite SnTiO_3 unit cell are $a = b = 5.0713$ Å, $c = 21.8803$ Å, $\alpha = \beta = 90^\circ$, and $\gamma = 120^\circ$. The crystal structure and lattice constants are in consistent with recent experimental measurement.^{18, 26} In terms of atomic arrangement, edge-sharing connected TiO_6 polyhedra forms continuous planar network with top and bottom O layers capped by Sn atoms (Fig. 1a). SnTiO_3 layers are stacked in an ABC manner, but other stack orders are also reported in experimental work.¹⁸ This layered structure, with Sn-Sn $5s$ orbital lone-pair interaction between adjacent layers, are nearly identical to that of SnO.

Ilmenite SnTiO_3 has an indirect band gap of 2.40 eV by HSE with the valence band edge (VBE) at Γ point (Fig. 1b). This band gap is appropriate for BEOL transistor application. Originating from the Sn^{2+} chemistry, the top valence band shows a strong dispersion and light effective hole masses with $m_x^* = 0.49 m_0$ and $m_z^* = 0.51 m_0$. The high band curvature and small effective hole mass along vertical stacking direction is unusual but coincide with that of SnO, where hole transport along stacking direction is even more efficient than the in-plane direction.^{9, 27} This suggest that Sn-Sn lone pair interaction in ilmenite SnTiO_3 , similar to SnO, offers a hole transport channel across the planes. Further electron-phonon coupling calculation reveals that the hole mobilities along in-plane and out-of-plane directions are 68.9 and 64.8 $\text{cm}^2/(\text{V}\cdot\text{s})$, respectively. Such decent mobility would be suitable for logic device application in vertical CMOS technology. Orbital projected density of states (DOS) shows that both Sn- $5s$ and O- $2p$ orbitals comprise the VBE states, in contrast to typical oxides where the VBM is almost completely contributed by O- $2p$ orbitals. Meanwhile, Ti- $3d$ orbital dominates the conduction band edge (CBE) states as shown in Fig. 1c. The band gap is therefore determined by the orbital energy difference between Ti- $3d$ and hybridized O- $2p$ /Sn- $5s$.

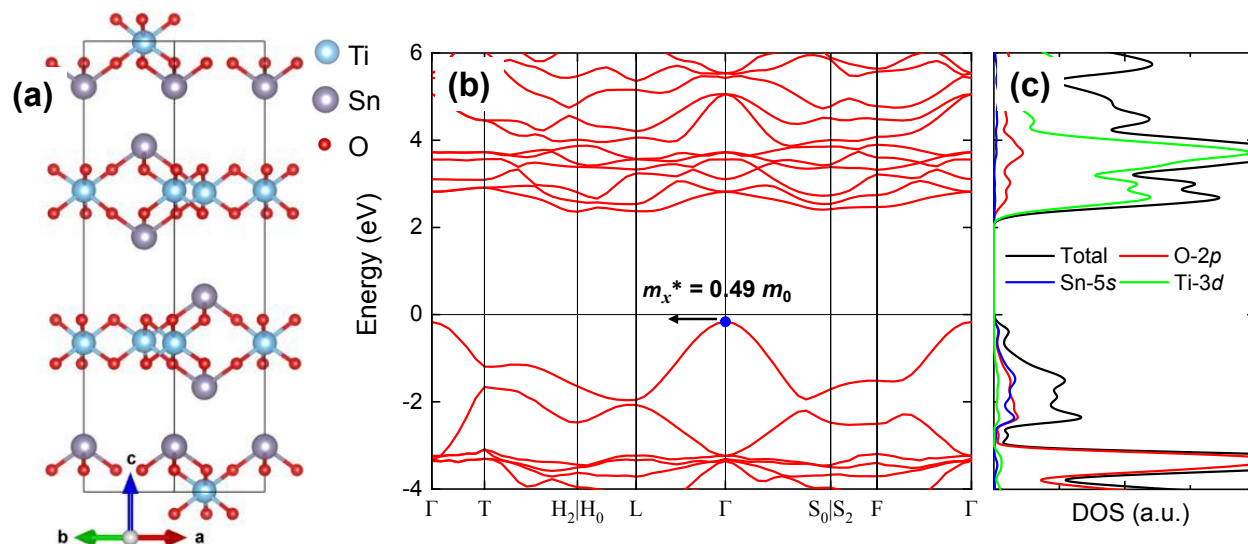


Figure 1. Crystal and electronic structure of ilmenite SnTiO_3 . (a) The atomic structure of ilmenite SnTiO_3 unit cell. (b) HSE calculated band structure of ilmenite SnTiO_3 . The band dispersion and effective hole mass along x -axis is indicated. (c) Total DOS and orbital projected DOS for O-2 p , Sn-5 s , and Ti-3 d in ilmenite SnTiO_3 .

The thermodynamical phase stability is an important figure-of-merit to consider as it determines p -type oxide long-term stability and synthesizability. In this work we evaluate SnTiO_3 phase stability from the chemical potential phase diagram.⁹ **Figure 2a** plots the phase stability region of ilmenite SnTiO_3 in Sn-Ti chemical potential space. SnTiO_3 perovskite phase with ferroelectricity does not appear in the phase diagram due to its metastable phase formation energy. This is consistent with numerous reports that the perovskite phase is challenging to synthesize and often it is resulted with the ilmenite phase.^{26, 28-30} Ilmenite SnTiO_3 occupies a small phase area, pointing to its less robust phase stability when comparing to other oxides like SnO_2 and TiO_2 . This is due to the fundamental issue of low stability Sn^{2+} valence state. Similar situation also happens to SnO with even narrower range of stability, $\Delta\mu_{\text{Sn}}$. Chemical potential phase diagram also provides information on materials synthesis condition. The elemental chemical potential depends on the growth environment such as temperature, partial pressure, and precursor concentration. From the phase diagram, a Sn-rich and Ti intermediate-rich condition is preferred for SnTiO_3 growth. Overall, we expect that SnTiO_3 could be synthesized and stably exist provided the elemental chemical potential condition is satisfied. Experimentally, atomic layer deposition (ALD) and molecular beam epitaxy (MBE) are the two possible methods to grow SnTiO_3 film. A reducing growth environment and controlled Ti/Sn precursor ratio are suggested to obtain SnTiO_3 ilmenite phase.

The chemical potential diagram is also necessarily for defect calculation as the defect formation energy depends on the chemical potential. Defects, especially hole-compensating defects, needs to be evaluated for accessing the hole dopability for p -type oxides. Oxides with spontaneous formed hole-compensating defects could not be p -type dopable. **Figure 2b** presents the calculated defect formation energy for both intrinsic defects and some possible extrinsic p -type dopants. The chemical potential used for defect calculation is oxygen rich condition (most favorable for p -type doping). Such condition corresponds to the boundary region in the phase diagram (red dot in

Figure 2a) where the oxygen chemical potential reaches the maximum. For oxygen rich condition, SnTiO_3 show no hole-compensating native defects as the oxygen vacancy presents sizable formation energy even at the limit of degenerating doping level (Fermi level approaching to the valence band edge). For a typical oxide, the anion vacancy (oxygen vacancy) is the potential hole-killer and cation vacancy is the possible electron-killer. The energy range over which both anion vacancy and cation vacancy are not spontaneously formed is the dopable energy range (**Figure 2b**). The dopability energy range is also called Fermi level pinning energy because the Fermi level cannot be shifted beyond this range. For ilmenite SnTiO_3 , its doping energy range covering the valence band edge suggests that it can be highly hole doped. We also calculated the effective density of states at VBM to estimate the maximum achievable hole doping concentration in SnTiO_3 . The calculated value is about $8.85 \times 10^{18} \text{ cm}^{-3}$ based on the Ref [31], which is high enough for SnTiO_3 to be a good semiconductor. We next consider possible *p*-dopants in SnTiO_3 . We investigate N substituting for O, K for Sn, and Sc for Ti as those dopants have comparable atomic size the one less valence electron than their respective host atoms. In **Figure 2b**, N replacing for O (N_O) and Sc for Ti (Sc_Ti) present accessible formation energy as well as shallow enough charge transition level. This suggests that N_O and Sc_Ti will be electrically active and donate holes in SnTiO_3 . We thus suggest N and Sc as the acceptors for achieving hole doping SnTiO_3 .

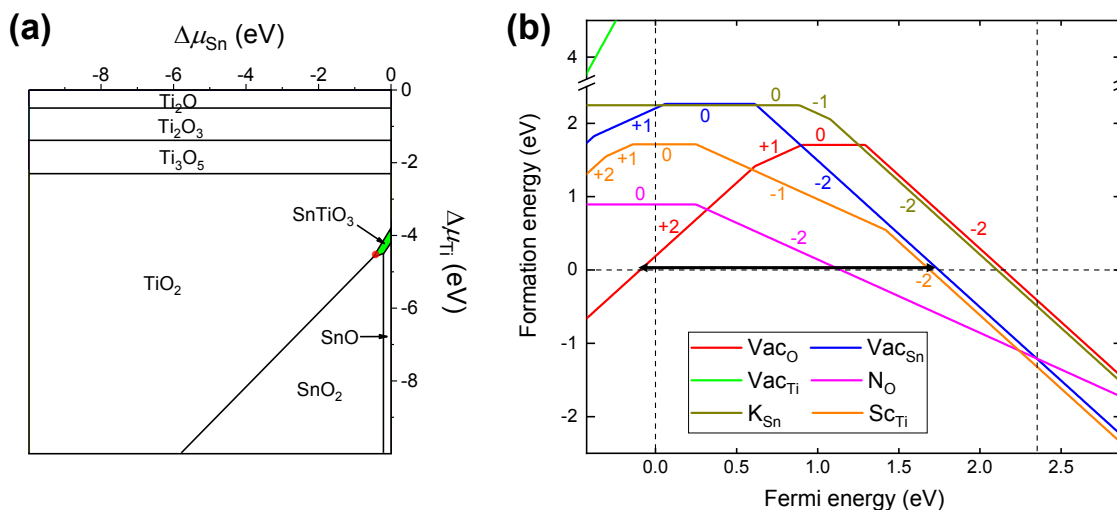


Figure 2. (a) Phase stability diagram of ilmenite SnTiO_3 calculated from first principles in terms of Sn-Ti chemical potential map. The green region of Sn-Ti chemical potentials indicates where ilmenite SnTiO_3 is thermodynamically stable. The oxygen-rich condition is indicated by a red dot. (b) Calculated formation energies of native defects and possible extrinsic *p*-dopants versus Fermi level in SnTiO_3 . The doping energy range is indicated by the horizontal arrowed line. Defect charge states are indicated. Valence band edge is shifted to 0 eV. VBE and CBE are indicated by vertical dashed lines.

The band alignment, i.e., VBE position relative to the vacuum level is determined by a slab model calculation. The bulk phase was firstly calculated to obtain the energy difference between the VBE and a core reference level (O-1s level in this work). A slab model was then calculated to obtain the energy difference between vacuum level and reference level. Two energy differences were then used to get the VBE position. It is found that the thickness of the slab model does not influence the calculated vacuum level and core reference level. For the slab model, two end surfaces must

be symmetric to obtain a flat potential level in the vacuum region. **Figure 3a** plots the planar averaged electrostatic potential of ilmenite $\text{SnTiO}_3(100)$ slab. The ionization potential (energy difference between VBE and vacuum level) is determined to be ~ 4.3 eV, which is quite shallow comparing with most other oxides (**Figure 3b**). The calculated ionization potential of SnTiO_3 is well consistent with recent work by Diehl et. al.¹⁹ The shallow VBE is due to the Sn-5s orbital hybridizing with O-2p and raising the VBE position. The calculated VBE of SnTiO_3 is very close to that of SnO (-4.0 eV), consistent with our atomic and electronic structure analysis that Sn-Sn lone pair interaction dominates the VBE states.

Valence band position is an important figure-of-merit for *p*-type oxides as it determines whether a *p*-type oxide is hole-dopable or not. Previous works by Robertson et. al.³² have generalized the correlation of native defects-limited *p*-type dopability to VBE position: *n*-type dopability requires deep conduction band edge (CBE below -4.5 eV, **Figure 3b**) and *p*-type dopability necessitates shallow VBE (VBE above -6.8 eV). A small ionization potential of 4.3 eV means the valence band of SnTiO_3 is well above the *p*-doping limit, suggesting its high *p*-type dopability. The shallow VBE position in SnTiO_3 also implies that it could form low Schottky barrier height with contact metals, leading to better contact performance for device application.

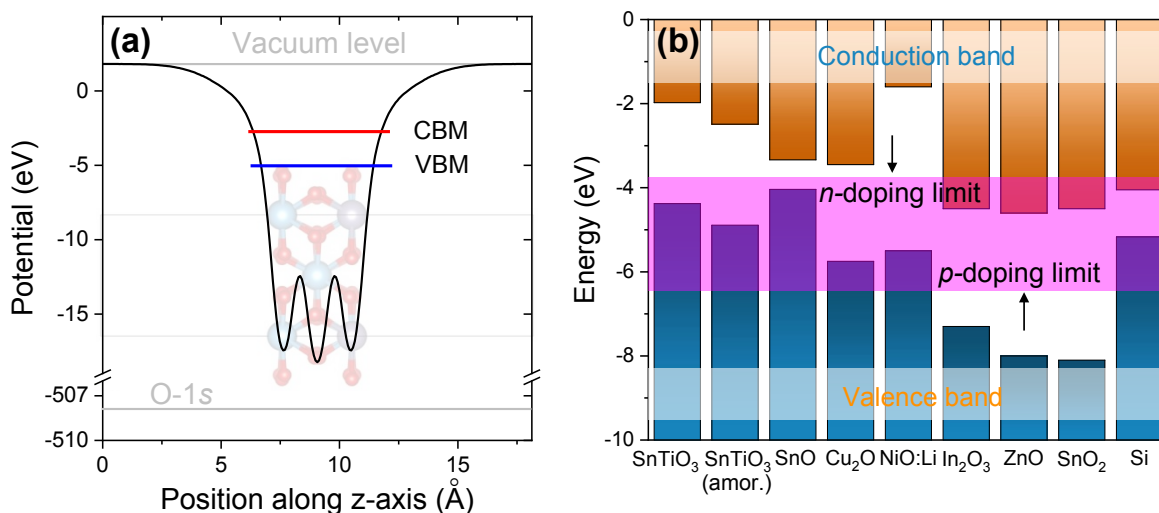


Figure 3. (a) Planar-averaged electrostatic potential of ilmenite $\text{SnTiO}_3(100)$ surface slab. Oxygen 1s core orbital energy level is used as common reference level for band alignment. Atomic structure of $\text{SnTiO}_3(100)$ surface slab is shown as an insert. Band edges (CBE/VBE) and O-1s core level are indicated. (b) Calculated band alignment of SnTiO_3 referenced to the vacuum level, together with other known *p*-type and *n*-type oxides. Band alignment for amorphous SnTiO_3 is also included (see next section). The dopable region is shaded with magenta color. The conduction and valence band edges should be located within this region for *n*-type and *p*-type dopability, respectively.

Oxide semiconductors for BEOL applications will assume amorphous phases due to low synthesis temperature. Therefore, it would be important to investigate the semiconducting performance of amorphous phase SnTiO_3 (*a*- SnTiO_3). *Ab-initio* molecular dynamics was performed to generate the atomic structure of *a*- SnTiO_3 by using the melt-quench method.^{23, 33, 34} **Figure 4a** shows one representative structural model of *a*- SnTiO_3 , together with different element pair radial distribution functions (RDF). The RDF of Sn-O and Ti-O pairs exhibit an initial sharp peak suggesting a

chemically short-range ordered system. For all pairs, the second order peaks are significantly broadened and oscillations of $g(r)$ damp out at distances greater than 5 Å, indicating the loss of long-range order and confirming the validity of the generated a -SnTiO₃. In terms of carrier transport, the amorphous structure disorders cause tail states in the electronic band structure and localization of electron wavefunction, which leads to a reduced mobility. To quantify the degree of electron localization, we have calculated the inverse participation ratio (IPR) which is defined as $IPR = N \sum |\psi(r_i)|^4 / (\sum |\psi(r_i)|^2)^2$,³⁵ where i is lattice site, N is the total number of lattice sites, and $\psi(r_i)$ is the electron wavefunction at site i . More localized state will have a larger IPR value. **Figure 4b** shows the calculated electronic density of states (DOS) and IPR for each of energy state in a -SnTiO₃. Comparing with crystalline SnTiO₃ (c -SnTiO₃), no obvious gap states appear in a -SnTiO₃. A mobility gap of 2.4 eV in a -SnTiO₃ is determined which is close to the crystalline phase band gap. In a previous work, a method was developed to predict an amorphous phase mobility model using IPR.³³ Based on this modelling method, the estimated hole mobility for a -SnTiO₃ stands at 29.2 cm²/Vs which is a decent value compared to currently investigated p -type oxides where mobility values typically range from 0.01~5 cm²/Vs.¹⁴ Similar to c -SnTiO₃, the band alignment of a -SnTiO₃ is determined by using slab model and the calculated VBE position is ~ 4.9 eV below the vacuum level (**Figure 4c**). The VBE position, though deeper than c -SnTiO₃ (~ 4.3 eV below the vacuum level), is located within the p -dopable range suggesting its p -type dopability. Shallow VBE would also allow a low Schottky barrier with contact metals. The intrinsic hole compensating defect V_O is further calculated to verify its p -type dopability. **Figure 4d** shows the formation energy of three representative O atoms with different coordination numbers (CN). In amorphous phase where each atom is unique, it is not feasible to access the vacancy formation energies of all O atoms. Here we use coordination number to group O atoms and investigate the formation energies of O vacancy from each CN group. In a -SnTiO₃, CN of O atom can be 2, 3, or 4. From **Figure 4d**, V_O from three CN groups all exhibit positive formation energies even when Fermi level approaches to the VBE. This indicates that V_O will not form spontaneously at high p -doping condition. The above results show that a -SnTiO₃ is experimentally realizable high-mobility hole dopable p -type oxide.

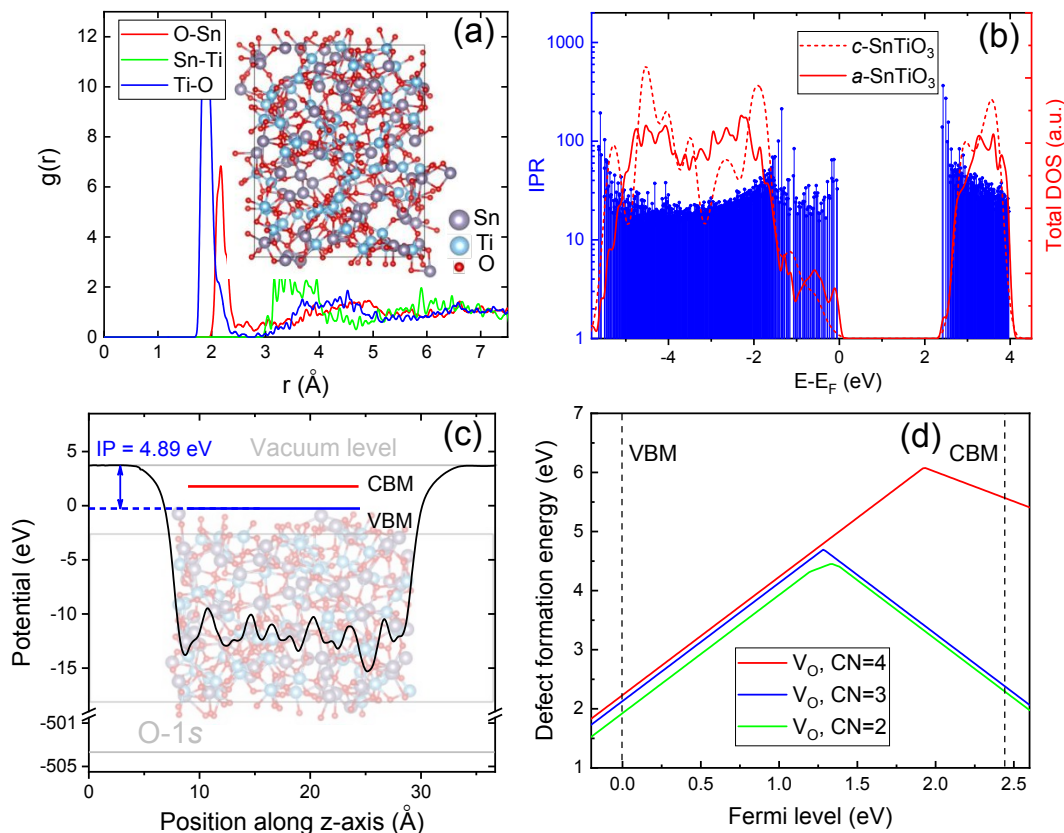


Figure 4. (a) Partial radial radial distribution function of O-Sn, Ti-O, and Sn-Ti pairs. A representative amorphous structure of SnTiO_3 generated by melt-quench method is shown as an insert. (b) Electronic density of states (DOS) and inverse participation ratio (IPR) of $a\text{-SnTiO}_3$. The DOS of $c\text{-SnTiO}_3$ is also plotted for comparison. (c) Planar-averaged electrostatic potential of $a\text{-SnTiO}_3(001)$ surface slab. Oxygen 1s core orbital energy level is used as common reference level for band alignment. The ionization potential (IP) is illustrated as the energy difference between vacuum level and VBE. Atomic structure of $a\text{-SnTiO}_3(001)$ surface slab is shown as an insert. (d) Calculated V_O formation energy versus Fermi level in $a\text{-SnTiO}_3$. Valence band edge is shifted to 0 eV. Three representative oxygen atoms with different CN are selected to investigate V_O formation energy in $a\text{-SnTiO}_3$. VBM and CBM are indicated by vertical lines.

IV. Conclusion

In conclusion, we have systematically investigated ilmenite and amorphous SnTiO_3 for p -type oxide application. As a Sn^{2+} based oxide, SnTiO_3 has $\text{Sn-}5s/\text{O-}2p$ orbital hybridization at its VBE states, which is the origin of high hole mobility. Electronic structure analysis shows that it has a wide band gap of 2.4 eV and high crystalline hole mobility of 68.9 and 64.8 $\text{cm}^2/(\text{V}\cdot\text{s})$ along in-plane and out-of-plane directions. Furthermore, the hole mobility of $a\text{-SnTiO}_3$ is predicted to be high, 29.2 $\text{cm}^2/(\text{V}\cdot\text{s})$. The wide band gap and high hole mobility render SnTiO_3 great promise for logic device application. Phase stability calculation reveals SnTiO_3 is a slightly robust phase but can be synthesized and stably exist given the suitable environment. Defect computation shows ilmenite SnTiO_3 can achieve high hole doping condition without spontaneous formed hole-killers. SnTiO_3 also presents a shallow VBE and can achieve good Ohmic contact to metals. These results

suggest ilmenite and amorphous SnTiO₃ is a promising experimentally realizable *p*-type oxide for future oxide electronics.

ACKNOWLEDGEMENT

This work was supported by ASCENT, one of the six centers in JUMP, a Semiconductor Research Corporation (SRC) program sponsored by Defense Advanced Research Projects Agency (DARPA).

Reference

1. Nomura, K.; Ohta, H.; Takagi, A.; Kamiya, T.; Hirano, M.; Hosono, H., Room-Temperature Fabrication of Transparent Flexible Thin-Film Transistors Using Amorphous Oxide Semiconductors. *nature* **2004**, 432 (7016), 488-492.
2. Ellmer, K., Past Achievements and Future Challenges in the Development of Optically Transparent Electrodes. *Nat. Photonics* **2012**, 6 (12), 809-817.
3. Fortunato, E.; Barquinha, P.; Martins, R., Oxide Semiconductor Thin-Film Transistors: A Review of Recent Advances. *Adv. Mater.* **2012**, 24 (22), 2945-2986.
4. Petti, L.; Münzenrieder, N.; Vogt, C.; Faber, H.; Büthe, L.; Cantarella, G.; Bottacchi, F.; Anthopoulos, T. D.; Tröster, G., Metal Oxide Semiconductor Thin-Film Transistors for Flexible Electronics. *Appl. Phys. Rev* **2016**, 3 (2), 021303.
5. Salahuddin, S.; Ni, K.; Datta, S., The Era of Hyper-Scaling in Electronics. *Nat. Electron* **2018**, 1 (8), 442-450.
6. Zhang, Z.; Hu, Y.; Lin, Z.; Si, M.; Charnas, A.; Cho, K.; Peide, D. Y., Atomically Thin Indium-Tin-Oxide Transistors Enabled by Atomic Layer Deposition. *IEEE Trans. Electron Devices* **2021**, 69 (1), 231-236.
7. Si, M.; Hu, Y.; Lin, Z.; Sun, X.; Charnas, A.; Zheng, D.; Lyu, X.; Wang, H.; Cho, K.; Ye, P. D., Why In₂O₃ Can Make 0.7 Nm Atomic Layer Thin Transistors. *Nano Lett.* **2020**, 21 (1), 500-506.
8. Hu, Y.; Hwang, J.; Lee, Y.; Conlin, P.; Schlom, D. G.; Datta, S.; Cho, K., First Principles Calculations of Intrinsic Mobilities in Tin-Based Oxide Semiconductors SnO, SnO₂, and Ta₂SnO₆. *J. Appl. Phys.* **2019**, 126 (18), 185701.
9. Hu, Y.; Yao, X.; Schlom, D. G.; Datta, S.; Cho, K., First Principles Design of High Hole Mobility P-Type Sn–O–X Ternary Oxides: Valence Orbital Engineering of Sn²⁺ in Sn²⁺–O–X by Selection of Appropriate Elements X. *Chem. Mater.* **2020**, 33 (1), 212-225.
10. Hautier, G.; Miglio, A.; Ceder, G.; Rignanese, G.-M.; Gonze, X., Identification and Design Principles of Low Hole Effective Mass P-Type Transparent Conducting Oxides. *Nat. Commun.* **2013**, 4 (1), 1-7.
11. Youn, Y.; Lee, M.; Kim, D.; Jeong, J. K.; Kang, Y.; Han, S., Large-Scale Computational Identification of P-Type Oxide Semiconductors by Hierarchical Screening. *Chem. Mater.* **2019**, 31 (15), 5475-5483.
12. Yim, K.; Youn, Y.; Lee, M.; Yoo, D.; Lee, J.; Cho, S. H.; Han, S., Computational Discovery of P-Type Transparent Oxide Semiconductors Using Hydrogen Descriptor. *Npj Comput. Mater.* **2018**, 4 (1), 1-7.
13. Kawazoe, H.; Yasukawa, M.; Hyodo, H.; Kurita, M.; Yanagi, H.; Hosono, H., P-Type Electrical Conduction in Transparent Thin Films of CuAlO₂. *Nature* **1997**, 389 (6654), 939-942.
14. Wang, Z.; Nayak, P. K.; Caraveo-Frescas, J. A.; Alshareef, H. N., Recent Developments in P-Type Oxide Semiconductor Materials and Devices. *Adv. Mater.* **2016**, 28 (20), 3831-3892.

15. Sato, H.; Minami, T.; Takata, S.; Yamada, T., Transparent Conducting P-Type Nio Thin Films Prepared by Magnetron Sputtering. *Thin Solid Films* **1993**, 236 (1-2), 27-31.
16. Ogo, Y.; Hiramatsu, H.; Nomura, K.; Yanagi, H.; Kamiya, T.; Hirano, M.; Hosono, H., P-Channel Thin-Film Transistor Using P-Type Oxide Semiconductor, Sno. *Appl. Phys. Lett.* **2008**, 93 (3), 032113.
17. Barone, M.; Foody, M.; Hu, Y.; Sun, J.; Frye, B.; Perera, S. S.; Subedi, B.; Paik, H.; Hollin, J.; Jeong, M., Growth of Ta₂sno₆ Films, a Candidate Wide-Band-Gap P-Type Oxide. *J. Phys. Chem. C* **2022**, 126 (7), 3764-3775.
18. Diehl, L.; Bette, S.; Pielnhofner, F.; Betzler, S.; Moudrakovski, I.; Ozin, G. A.; Dinnebier, R.; Lotsch, B. V., Structure-Directing Lone Pairs: Synthesis and Structural Characterization of Sntio₃. *Chem. Mater.* **2018**, 30 (24), 8932-8938.
19. Diehl, L.; Fabini, D. H.; Vargas-Barbosa, N. M.; Jimenez-Solano, A.; Block, T.; Duppel, V.; Moudrakovski, I.; Küster, K.; Pöttgen, R.; Lotsch, B. V., Interplay between Valence Band Tuning and Redox Stability in Sntio₃: Implications for Directed Design of Photocatalysts. *Chem. Mater.* **2021**, 33 (8), 2824-2836.
20. Blöchl, P. E., Projector Augmented-Wave Method. *Phys. Rev. B* **1994**, 50 (24), 17953.
21. Paier, J.; Marsman, M.; Hummer, K.; Kresse, G.; Gerber, I. C.; Ángyán, J. G., Screened Hybrid Density Functionals Applied to Solids. *J. Chem. Phys.* **2006**, 124 (15), 154709.
22. Sung, H.-J.; Mochizuki, Y.; Oba, F., Surface Reconstruction and Band Alignment of Nonmetallic a (Ii) B (Iv) O₃ Perovskites. *Phys. Rev. Mater.* **2020**, 4 (4), 044606.
23. Hu, Y., Amorphous Ta₂sno₆: A Hole-Dopable P-Type Oxide. *Submitted*.
24. Freysoldt, C.; Neugebauer, J.; Van de Walle, C. G., Electrostatic Interactions between Charged Defects in Supercells. *Phys. Status Solidi B* **2011**, 248 (5), 1067-1076.
25. Broberg, D.; Medasani, B.; Zimmermann, N. E.; Yu, G.; Canning, A.; Haranczyk, M.; Asta, M.; Hautier, G.; Pycdt: A Python Toolkit for Modeling Point Defects in Semiconductors and Insulators. *Comput. Phys. Commun.* **2018**, 226, 165-179.
26. Fix, T.; Sahonta, S.-L.; Garcia, V.; MacManus-Driscoll, J. L.; Blamire, M. G., Structural and Dielectric Properties of Sntio₃, a Putative Ferroelectric. *Cryst. Growth Des.* **2011**, 11 (5), 1422-1426.
27. Hu, Y., Interlayer Engineering of Band Gap and Hole Mobility in P-Type Oxide Sno. *ACS Appl. Mater. Interfaces*. accepted.
28. O'Donnell, S.; Chung, C.-C.; Carbone, A.; Broughton, R.; Jones, J. L.; Maggard, P. A., Pushing the Limits of Metastability in Semiconducting Perovskite Oxides for Visible-Light-Driven Water Oxidation. *Chem. Mater.* **2020**, 32 (7), 3054-3064.
29. Pielnhofner, F.; Diehl, L.; Jiménez-Solano, A.; Bussmann-Holder, A.; Schön, J. C.; Lotsch, B. V., Examination of Possible High-Pressure Candidates of Sntio₃: The Search for Novel Ferroelectric Materials. *APL Mater* **2021**, 9 (2), 021103.
30. Chung, H. K.; Pyeon, J. J.; Baek, I.-H.; Lee, G.-Y.; Lee, H.; Won, S. O.; Han, J. H.; Chung, T.-M.; Park, T. J.; Kim, S. K., Investigation of Phases and Chemical States of Tin Titanate Films Grown by Atomic Layer Deposition. *J. Vac. Sci. Technol.* **2020**, 38 (1), 012404.
31. <https://www.iue.tuwien.ac.at/phd/palankovski/node41.html>, accessed on Feb 12, 2023.
32. Robertson, J.; Clark, S., Limits to Doping in Oxides. *Phys. Rev. B* **2011**, 83 (7), 075205.
33. Lee, Y.; Hu, Y.; Kim, D.; Datta, S.; Cho, K., First-Principles Mobility Prediction for Amorphous Semiconductors. *Phys. Rev. B* **2022**, 105 (8), 085201.
34. Buchholz, D. B.; Ma, Q.; Alducin, D.; Ponce, A.; Jose-Yacaman, M.; Khanal, R.; Medvedeva, J. E.; Chang, R. P., The Structure and Properties of Amorphous Indium Oxide. *Chem. Mater.* **2014**, 26 (18), 5401-5411.
35. Kaur, K.; Singh, C. V., Amorphous Tio₂ as a Photocatalyst for Hydrogen Production: A Dft Study of Structural and Electronic Properties. *Energy Procedia* **2012**, 29, 291-299.